JOURNAL OF GUIDANCE, CONTROL, AND DYNAMICS
Vol. 19, No. 6, November–December 1996

Preliminary Study of Optimal Thrust-Limited Path-Constrained Maneuvers

Russel S. Wenzel*
Lockheed Martin Missiles and Space Company, Inc., Sunnyvale, California 94088-3504
and
John E. Prussing†
University of Illinois at Urbana–Champaign, Urbana, Illinois 61801-2935

Fuel-optimal maneuvers of a constant-specific-impulse, thrust-limited spacecraft in field-free space are analyzed. The simple problem of an optimal maneuver from a state of rest at one location to a state of rest at another location becomes very complex when a path constraint is introduced. Solutions are obtained using a direct numerical optimization method that combines Hermite–Simpson transcription and nonlinear programming. The resulting Lagrange multipliers provide a discrete approximation to the primer vector. The necessary conditions for an optimal solution can then be checked to validate the solution. Fundamental concepts, such as the existence of boundary arcs or boundary points and the optimal number of coast arcs, are examined. A comprehensive solution is obtained for symmetric rest-to-rest maneuvers. More general maneuvers are also examined.

Introduction

OPTIMAL spacecraft trajectory problems typically consider time and terminal constraints, but not interior path constraints.[1–4] Path constraints for impulsive trajectories have been investigated by several authors[5–9] and various necessary conditions for an optimal constrained solution have been found. Comprehensive solutions for the impulsive, path-constrained problem in the two-body, inverse-square gravitational field and for field-free space have been obtained,[10,11] but, to the authors' knowledge, no comprehensive solution for constant-specific-impulse, thrust-limited trajectories has been presented.

The problem is interesting because of its practical application and also because of the extreme complexity of the solution compared with the simple solution in the absence of the path constraint. This simple unconstrained solution is presented in the Appendix.

In an analytical study, Groble[12] identified some preliminary characteristics of optimal thrust-limited, path-constrained solutions in field-free space. However, to obtain an analytical solution to the associated Euler–Lagrange two-point boundary value problem, certain assumptions were made on the geometric form of the solution, limiting its generality. By utilizing the direct numerical technique of Hermite–Simpson transcription in conjunction with nonlinear programming, these limitations are avoided and a comprehensive solution to the problem is obtained.[13]

Problem Statement

It is desired to minimize the propellant consumption of a constant-specific-impulse, thrust-limited spacecraft maneuvering between specified terminal conditions in field-free space. The final position and velocity are to be achieved within a specified final time. Additionally, the position of the spacecraft is constrained to lie outside a closed, inadmissible region of space.

As a simple example, consider the motion of a spacecraft traveling in field-free space from rest to rest in a plane and restricted to the region outside of a circle of specified radius. A practical application of such a constraint is a safe operating region around a large space structure or celestial body, such as an asteroid. It is convenient to refer all motion to a Cartesian frame of reference having its origin at the center of the circular constraint, as shown in Fig. 1.

Because the only force acting on the spacecraft is its thrust, the equation of motion of the spacecraft is

$$\dot{\boldsymbol{r}} = \boldsymbol{v} \tag{1}$$

$$\dot{\boldsymbol{v}} = \Gamma \boldsymbol{u} \tag{2}$$

where $\boldsymbol{r}$ and $\boldsymbol{v}$ are the spacecraft position and velocity vectors, Γ is the thrust acceleration of the spacecraft engine, and $\boldsymbol{u}$ is a unit vector in the direction of the thrust, where $\boldsymbol{u}^T = [\cos\theta \ \sin\theta]$ in terms of the thrust angle θ depicted in Fig. 1.

A cost functional representing the amount of propellant consumed by a constant specific impulse engine is given by[14]

$$J = \int_{t_0}^{t_f} \Gamma \, dt \tag{3}$$

The complete problem may now be stated as minimizing the cost J in Eq. (3) by the choice of the thrust acceleration magnitude

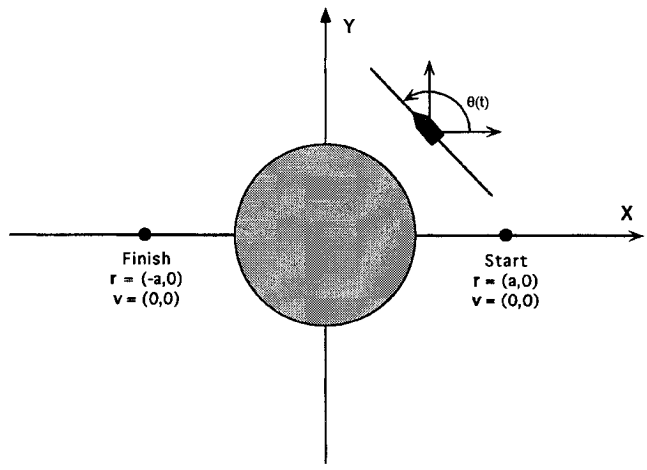

Fig. 1 Rendezvous geometry for the symmetric, rest-to-rest case.

Presented as Paper AAS 91-133 at the AAS/AIAA Spaceflight Mechanics Meeting, Houston, TX, Feb. 11–13, 1991; received July 9, 1995; revision received July 2, 1996; accepted for publication July 21, 1996.

*Senior Research Engineer, Department 73-17 B/150.
†Professor, Department of Aeronautical and Astronautical Engineering. Fellow AIAA.

$\Gamma(t)$ and direction $\theta(t)$, subject to various constraints, including the equations of motion

$$\dot{x} = \begin{bmatrix} \dot{r} \\ \dot{v} \end{bmatrix} = \begin{bmatrix} v \\ \Gamma u \end{bmatrix} = \begin{bmatrix} x_3 \\ x_4 \\ \Gamma \cos\theta \\ \Gamma \sin\theta \end{bmatrix} \tag{4}$$

and specified initial and final states $x(t_0) = x_0$ and $x(t_f) = x_f$. For the results presented the initial and final velocities are zero. There is a path constraint

$$r = \left(x_1^2 + x_2^2\right)^{\frac{1}{2}} \geq r_c \tag{5}$$

and the maneuver time constraint

$$t_f - t_0 \leq t_{\max} \tag{6}$$

where $t_{\max}$ is specified, and the bounds on the thrust acceleration

$$0 \leq \Gamma \leq \Gamma_{\max} \tag{7}$$

Without loss of generality, let the initial time $t_0 = 0$ and choose units such that $r_c = 1$ and $\Gamma_{\max} = 1$. This defines a set of canonical units. Assuming a constant value for the maximum thrust acceleration, as opposed to the maximum thrust, is a simplifying approximation in this preliminary investigation that alleviates having to keep track of the change in mass. This constant mass approximation is valid if the propellant mass is a small fraction of the total vehicle mass.

The optimal control problem described by Eqs. (1–3) subject to constraints (5–7) was examined by Groble,[12] and some preliminary results were obtained analytically for rest-to-rest symmetric rendezvous. The optimal thrust direction is the direction of the primer vector[1,14] $p(t)$, with the magnitude of the optimal thrust acceleration being given by

$$\Gamma(t) = \begin{cases} 1 & \text{if} \quad p > 1 \\ 0 & \text{if} \quad p < 1 \\ \text{intermediate} & \text{if} \quad p \equiv 1 \end{cases} \tag{8}$$

In field-free space the primer vector has the form

$$p(t) = p_0(t) + \dot{p}t \tag{9}$$

where the primer vector rate $\dot{p}$ is constant unless the path constraint becomes active, in which case a discontinuity may occur. Results obtained by Groble include the following.

1) A single boundary-arc (BA) type solution, in which the second burn arc of a three-burn trajectory coincides with the circular constraint surface, occurs when the initial position is $r_0^T = (1.740602354434, 0)$ for a maneuver time equal to 5.0812149488 and a cost of 3.186654046, under maximum thrust acceleration.

2) In cases for which the initial distance and maneuver time are sufficient to produce a single tangency point on the constraint surface [defined as a boundary point (BP)], the following hold true.

a) The BP occurs at (0, 1) at a time equal to half of the total maneuver time.

b) The Hamiltonian function for the optimal control problem is constant throughout the maneuver and is continuous at the BP.

c) The primer vector rate is discontinuous at the BP. This implies that the time rate of change of the optimal thrust acceleration is also discontinuous at the BP.

Numerical Method of Solution

A direct method of solution by Enright and Conway[15] is used to solve the optimal control problem utilizing Hermite–Simpson transcription and nonlinear programming (NLP). This is a variant of a method introduced by Hargraves and Paris.[16] It is a direct method in the sense that it does not explicitly solve the necessary conditions of optimality and the associated two-point boundary value problem. Instead, the state and control variables are discretized to form a parameter optimization problem. The resulting NLP problem is then solved numerically, and the continuous solution including the primer vector is reconstructed through an approximation process using the Lagrange multipliers from the NLP solution. The transformation of the infinite-dimensional, continuous problem to the finite-dimensional, parameter problem is called transcription. The method employed here is to use Hermite interpolation with Simpson integration to transcribe the differential equations of motion into nonlinear constraints in the NLP solution. This results in an implicit Hermite–Simpson integration of the equations of motion.

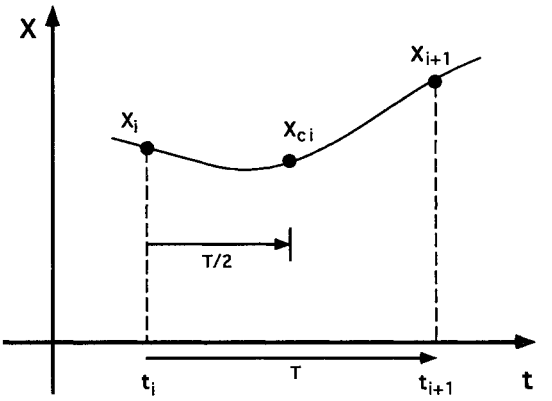

Fig. 2 Time segment for Hermite–Simpson integration.

It is desired to approximate the solution to the differential equation

$$\dot{x} = f(x, t) \tag{10}$$

on an interval $t_i \leq t \leq t_{i+1}$.

Let the state vector $x(t)$ be approximated by a Hermite cubic polynomial, determined by the values and slopes at the endpoints of the interval of length $T = t_{i+1} - t_i$ as shown in Fig. 2. By normalizing the time interval so that $t = sT$, where $0 \leq s \leq 1$, the Hermite interpolant can be shown to have the following form[13]:

$$x(s) = x_i(s-1)^2(2s+1) + Tf(x_i, t_i)s(s-1)^2 + x_{i+1}s^2(3-2s) + Tf(x_{i+1}, t_{i+1})s^2(s-1) \tag{11}$$

Once having obtained the interpolant, a Simpson quadrature rule is used to obtain the implicit integration formula

$$x_{i+1} = x_i + (T/6)[f(x_i, t_i) + 4f(x_{ci}, t_{ci}) + f(x_{i+1}, t_{i+1})] \tag{12}$$

where $t_{ci} = t_i + T/2$, and x_{ci} is found by evaluating the interpolant at $s = \frac{1}{2}$

$$x_{ci} = x\left(\tfrac{1}{2}\right) = \tfrac{1}{2}(x_i + x_{i+1}) + (T/8)[f(x_i, t_i) - f(x_{i+1}, t_{i+1})] \tag{13}$$

Equation (12) is clearly implicit and can justifiably be called the implicit Hermite–Simpson integration formula. In transcription, a set of defect vectors is defined. If x_i, x_{i+1}, and t_i, t_{i+1} are determined by some process, the error (defect) resulting from Eq. (12) can be measured by subtracting x_{i+1} from both sides of Eq. (12) to yield

$$\Delta_i \equiv x_i - x_{i+1} + (T/6)[f(x_i, t_i) + 4f(x_{ci}, t_{ci}) + f(x_{i+1}, t_{i+1})] \tag{14}$$

It is through the defect equation (14) that the equations of motion (4) are transcribed into nonlinear constraints that are driven to zero to approximately satisfy the equations of motion.

Discretization Process and NLP Problem Formulation

It is desired to transcribe the following continuous optimal control problem[17]: determine the control $u(t)$, the final time t_f, and the resulting trajectory $x(t)$ that minimizes

$$J \equiv \phi[x(t_f), t_f] + \int_0^{t_f} L[x(t), u(t), t]\,dt \tag{15}$$

subject to the differential equation of motion with initial conditions

$$\dot{x} = f[x(t), u(t), t]; \qquad x(0) = x_0 \tag{16}$$

the terminal constraints

$$\Psi[x(t_f), t_f] = 0 \tag{17}$$

and the state inequality (path) constraint

$$S[\boldsymbol{x}(t), t] \leq 0 \tag{18}$$

where the state $\boldsymbol{x}(t) \in R^n$, control $\boldsymbol{u}(t) \in R^m$, and terminal constraint $\Psi \in R^q$.

The discretization process is performed in the following manner. Introduce $N+1$ partitions of time $\{t_1, t_2, \ldots, t_{N+1}\}$ of uniform length $T = (t_f - t_0)/N$, where $t_1 = 0$ and $t_{N+1} = t_f$. The mesh points t_i are called nodes, and the intervals $[t_i, t_{i+1}]$ are called segments. Let $\boldsymbol{x}_i$ and $\boldsymbol{u}_i$ represent the discretized values of the state and control vectors $\boldsymbol{x}(t_i)$ and $\boldsymbol{u}(t_i)$ at the ith node. By utilizing the vector form of the Hermite–Simpson defect equation (14), an equivalent discretized parameter optimization problem results: determine the control values $\{\boldsymbol{u}_1, \boldsymbol{u}_2, \ldots, \boldsymbol{u}_{N+1}\}$, the final time t_f, and the state values $\{\boldsymbol{x}_1, \boldsymbol{x}_2, \ldots, \boldsymbol{x}_{N+1}\}$ that minimize

$$J = \phi(\boldsymbol{x}_{N+1}, t_{N+1}) + T \sum_{i=1}^{N+1} w_i L(\boldsymbol{x}_i, \boldsymbol{u}_i, t_i) \tag{19}$$

subject to

$$\Delta_i = \boldsymbol{0} \qquad i = 1, \ldots, N+1 \tag{20}$$

$$\boldsymbol{x}_1 = \boldsymbol{x}_0 \tag{21}$$

$$\Psi(\boldsymbol{x}_{N+1}, t_{N+1}) = \boldsymbol{0} \tag{22}$$

$$S(\boldsymbol{x}_i, t_i) \leq 0 \tag{23}$$

The Hermite–Simpson defects are defined between nodes i and $i+1$ as

$$\Delta_i = \boldsymbol{x}_i - \boldsymbol{x}_{i+1} + (T/6)[\boldsymbol{f}(\boldsymbol{x}_i, \boldsymbol{u}_i, t_i) + 4\boldsymbol{f}(\boldsymbol{x}_{ci}, \boldsymbol{u}_{ci}, t_{ci}) + \boldsymbol{f}(\boldsymbol{x}_{i+1}, \boldsymbol{u}_{i+1}, t_{i+1}] \tag{24}$$

with the state, control, and time at the segment centers given by

$$\boldsymbol{x}_{ci} = \tfrac{1}{2}(\boldsymbol{x}_i + \boldsymbol{x}_{i+1}) + (T/8)[\boldsymbol{f}(\boldsymbol{x}_i, \boldsymbol{u}_i, t_i) - \boldsymbol{f}(\boldsymbol{x}_{i+1}, \boldsymbol{u}_{i+1}, t_{i+1})] \tag{25}$$

$$\boldsymbol{u}_{ci} = \tfrac{1}{2}(\boldsymbol{u}_i + \boldsymbol{u}_{i+1}) \tag{26}$$

$$t_{ci} = t_1 + (i-1)T/2 \tag{27}$$

Equations (19–23) now formulate the parameter optimization problem. The integral term in the cost functional of the continuous optimal control problem has been approximated by a quadrature rule, where w_i is a weighting parameter associated with the ith node for the particular quadrature rule utilized. Note that the control is approximated by a linear interpolant; alternate control interpolants are possible.[13]

When using a Lagrange-type NLP solver, the Lagrange multipliers associated with the nonlinear constraints are typically available. This presents an additional benefit of using Hermite–Simpson transcription: the Lagrange multipliers associated with the defect constraints are discrete approximations of the costate variables at the segment center.[15]

After the solution to the NLP problem is obtained by this direct method, the necessary conditions for optimality are checked to validate the solution. Hermite interpolation is used to approximate the costates at the interior nodes, and the variables at the initial and terminal nodes are determined by second-order Runge–Kutta integration. The Lagrange multipliers representing the velocity costate variables provide discrete representations of the primer vector components and provide invaluable information for validating the optimal solutions through Eqs. (8) and (9). As shown in the numerical results, the primer vector rate is discontinuous when the trajectory makes contact with the path constraint, as it should be.[17] The primer rate components are the position costate variables.

Computer Implementation

A Fortran program was written that implements the Hermite–Simpson transcribed rendezvous problem in a manner that utilizes the sequential quadratic programming NLP solver NPSOL[18] on a Convex 240 supercomputer. The problem is characterized by a three-burn-arc trajectory with two intermediate coast arcs. A direct method requires an initial structure for the solution. The method will not add burn arcs that are not there initially, but it will remove unnecessary burn arcs. This is the reason that three burn arcs was assumed, rather than two. The exact structure of the solution is not known a priori, but, as will be shown, this is the optimal number of burns and coast arcs as validated using the necessary conditions from primer vector theory. The first and third burn arcs are divided into six segments, and thus require seven nodes. To allow for the possibility that the second burn arc is longer than the other two, it contains 10 segments and, hence, 11 nodes. The resulting trajectory segmentation is shown in Fig. 3 and consists of a total of 22 segments and 25 nodes.

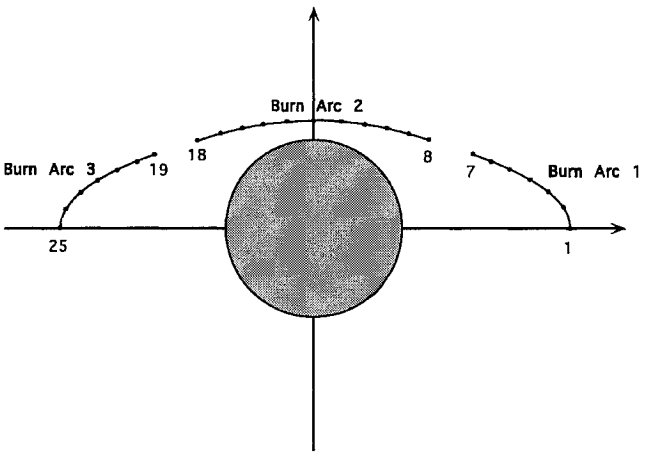

Fig. 3 Trajectory segmentation and nodal distribution.

A linear control structure is used instead of an alternate form because primer rate discontinuities (and hence control rate discontinuities in Γ and θ) are expected to occur on the optimal trajectory, corresponding to constraint surface contacts (BPs). The use of higher-order control structures such as cubic splines would require continuity of slope, and any discontinuities would have to be artificially added at a phase boundary.[15] The linear control structure further affords the NLP solver a savings in problem size. In addition, the Jacobian is close to diagonal, which is a numerical convenience.

Each node contains the 4 state variables (x_1, x_2, x_3, x_4) and 2 control variables (Γ, θ). The resulting NLP problem size is 153 variables and 140 constraints. The variables are

$$\boldsymbol{x}^T = \left[\boldsymbol{x}_1^T, \boldsymbol{u}_1^T, \boldsymbol{x}_2^T, \boldsymbol{u}_2^T, \ldots, \boldsymbol{x}_{25}^T, \boldsymbol{u}_{25}^T, t_1, t_2, t_3\right] \tag{28}$$

where t_1, t_2, and t_3 represent the burn arc (phase) durations. A trapezoidal rule is used in the objective function formulation in Eq. (19). Constraint gradients are also determined numerically as required. After the converged NLP solution is achieved, a post-processing code then reconstructs the entire state, costate, and control histories through the appropriate approximation structure.

A feasible initial trajectory is obtained by selecting the node locations to satisfy the path constraint. The most difficult aspect of the numerical solution is determining the minimum-time optimal trajectory. Once this is obtained it can be used as an initial guess for a longer transfer time trajectory as part of a numerical continuation method of solution to obtain all of the optimal trajectories. For these trajectories the run times were less than a minute. A cycloid shape was used as the initial guess for the minimum-time solution.

Computations were performed in double precision, resulting in 15 decimal digits of precision. There are no existing solutions to validate the numerical results, but the version of NPSOL used has four true–false flags.[18] These verify that 1) the projected gradient is small, 2) the active constraint residuals are small, 3) the multipliers indicate optimality, and 4) the last change in the parameter vector was small.

Numerical Results

The computer program developed is sufficiently general to solve any feasible rendezvous problem of this type, and an example

solution of a maneuver between arbitrary states is presented. However, a comprehensive solution is obtained for rest-to-rest rendezvous in the vicinity of the constraint and compared with known results whenever possible. A complete catalog of results is given in Ref. 13.

One fundamental property becomes immediately apparent, namely, that the optimal maneuver time is always the maximum allotted maneuver time. Hereafter the term maneuver time t_f is synonymous with the maximum allotted maneuver time t_{max} prescribed in the problem formulation.

Symmetric Rest-to-Rest Rendezvous

Figure 4 displays the characteristic regions for optimal solutions resulting from NLP solutions for a wide range of initial/terminal positions and maneuver times. Region I (shaded) represents infeasible cases for which the maximum thrust acceleration magnitude is insufficient to maneuver the vehicle from start to finish in the allotted time. The boundary separating region I from regions II and III represents minimum-time solutions, for which one continuous burn arc at maximum thrust is barely sufficient to complete the maneuver in the allotted time. For these solutions the cost is equal to the maneuver time, as seen from Eq. (3) because $\Gamma = 1$ throughout the maneuver. The trajectory and the optimal thrust direction for a maneuver of this type is shown in Fig. 5, which lies on the boundary separating regions I and II.

Region II Solutions

For solutions in region II of Fig. 4 the vehicle contacts the constraint surface at a single BP located at (0, 1) at a time equal to half the maneuver time, as shown in Fig. 5. The thrust acceleration magnitude has its maximum value of unity on all burn arcs. It is evident from Fig. 4 that this region does not extend over as broad an area as the other regions, and ceases to exist when the initial position is closer than approximately 1.21 from the origin. This is in excellent agreement with the result of Groble,[12] where this threshold was determined to lie at 1.211419.

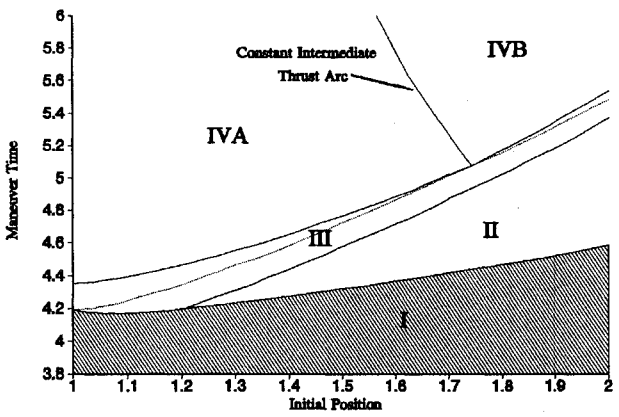

Fig. 4 Solution characteristic regions for symmetric, rest-to-rest case.

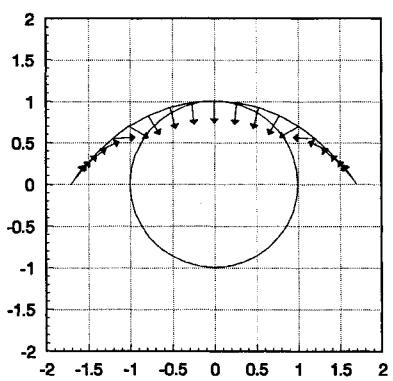

Fig. 5 Trajectory and thrust direction for minimum-time solution with initial position = 1.7 and cost = 4.422168.

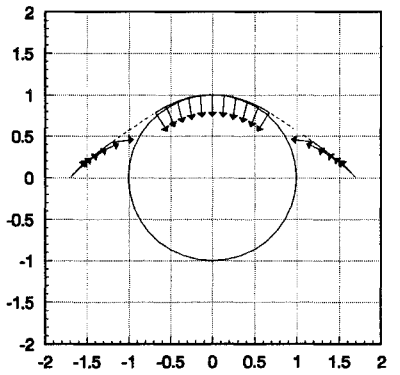

Fig. 6 Trajectory and thrust direction for initial position = 1.7, maneuver time = 4.75, and cost = 3.609455.

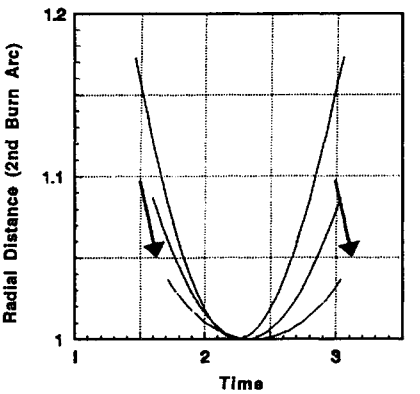

a) Radial distance on second burn arc

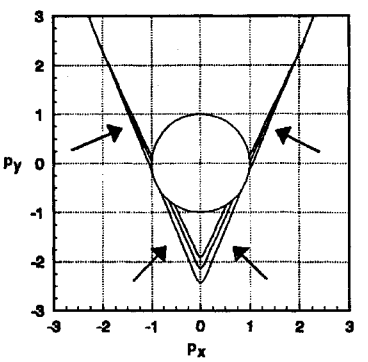

b) Primer vector plot

Fig. 7 Region II type solutions with initial position = 1.7 and maneuver time of 4.5 and larger (arrows show direction of increasing maneuver time).

Figures 6 and 7 display representative region II solutions. Of particular interest is Fig. 7, which displays two of the most informative trajectory characteristics: radial distance and primer vector history. Three values of maneuver time are shown. The thrust acceleration magnitude on all of the trajectories is determined to be constant and equal to unity. In Fig. 7a the radial distance for the second burn arc clearly shows a single BP at midtime.

In Fig. 7b the necessary conditions on the primer vector, Eqs. (8) and (9), are verified. By plotting the numerically generated primer vector on top of a unit circle, as expanded in Fig. 8, the complete thrust history is obtained. The engine is on at maximum thrust when the tip of the primer vector lies outside the unit circle, and the engine is off when it lies inside, as specified by Eq. (8). The thrust direction is also shown as the direction of the primer vector. The fact that the primer vector varies at a constant rate under an inactive path constraint, as specified by Eq. (9), is also evident from the straight line locus of the tip of the primer vector. Finally, the single discontinuity of the primer rate corresponding to the active path constraint, in the

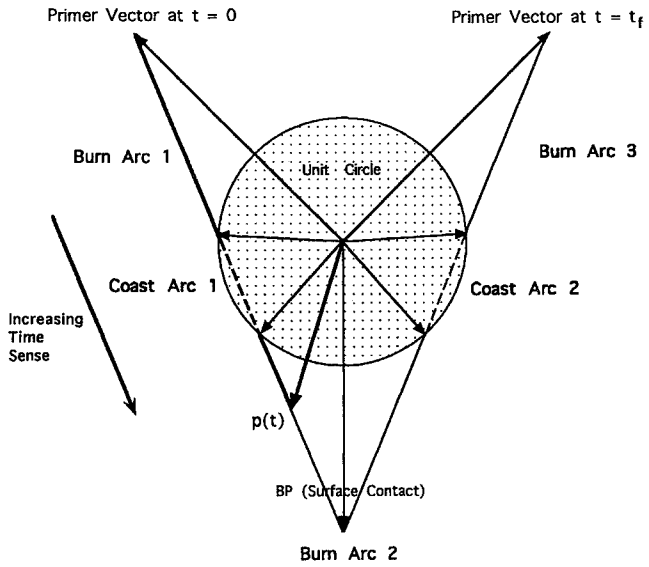

Fig. 8 Primer vector plot.

form of the BP at (0,1) is also apparent from Fig. 8. The form of the primer history shown agrees with the analytical form determined by Groble.[12]

The Hamiltonian function is also computed. It should be constant on the optimal solution except for possible discontinuities at instants when the path constraint becomes active.[17] It is determined to be constant except for a single spike at the midtime that can be attributed to the interpolation error caused by costate rate discontinuities at the time of contact with the constraint.

Region III Solutions

Region III type solutions can best be described as transitional. Solutions classified as this type occupy the narrow strip in the maneuver time and initial-position plane that separates regions I and II from region IV in Fig. 4. Region III is further partitioned by a line separating the region into two subregions. This line represents the minimum maneuver time for a particular initial position at which an intermediate thrust arc (ITA) develops on the second burn arc. Along an ITA the primer magnitude is $p \equiv 1$ and the ITA magnitude and direction are simply those required to ride the constraint boundary.

The entirety of region III, regardless of subregion, is characterized by the existence of multiple (two or more) points at which the trajectory contacts the constraint surface. This phenomenon is hereafter referred to as multiple BP behavior. As one might expect, these contact points occur only on the second burn arc, and their locations on the constraint surface change when the maneuver time is varied. The pattern by which BP locations vary with maneuver time can be determined by identifying which node or segment center has an active path constraint. On Lagrangian-based optimal NLP solutions, all active inequality constraints must have nonzero associated Lagrange multipliers, in contrast with the inactive constraints, which have zero multipliers.[19] Therefore, examination of the path constraint multiplier associated with each node and segment center indicates whether or not contact with the constraint surface has occurred. Further, if all node and/or segment center path constraint multipliers are nonzero, BA-type of solution is indicated.

To fully understand the transition from region III characteristics to region IV, one can fix the initial position and examine increasing values of maneuver time. A complication arises, however, because the transition develops differently depending on whether the initial position is less than, equal to, or greater than approximately 1.7406, the critical value determined by Groble[12] for the BA case.

Figure 9 displays a family of solutions with initial position at 1.3 and various maneuver times, typifying the transitional characteristics of all region III solutions with initial position less than 1.7406. Figure 9a displays a matrix of active path constraint Lagrange multipliers for all 11 nodes and 10 segment centers (21 total) on the second burn arc. An × indicates that the path constraint is active for

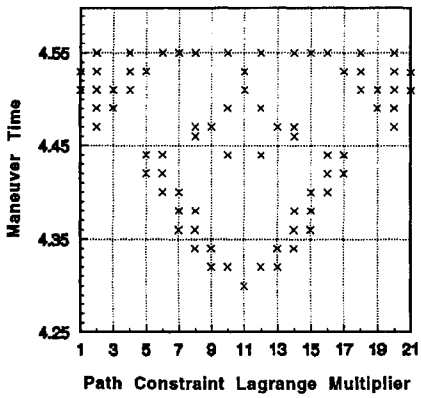

a) Active path constraints

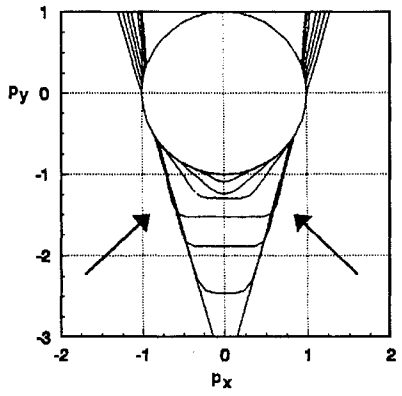

b) Primer vector plot

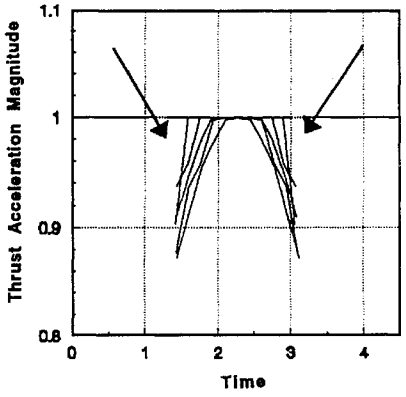

c) Thrust acceleration magnitude

Fig. 9 Region III type solutions with initial distance = 1.3 and increasing maneuver time.

that particular maneuver time. As maneuver time increases, the BPs, which start as a single BP at (0, 1), slide down the constraint surface on both sides and form ever longer finite duration BAs on each end of the second burn arc. Eventually, a full BA develops. This BP behavior is also shown in the other plots of Fig. 9. The single primer rate discontinuity of a region II solution develops into two and then more rate discontinuities, as seen in the primer vector plot in Fig. 9b, until ITAs begin to form on each end. Eventually, the entire second burn arc coincides with the unit circle, representing a full ITA.

As shown in Eq. (8) the possibility exists for an ITA if $p \equiv 1$. This is shown in Fig. 9c with the thrust acceleration magnitude being less than the maximum of unity as the ITAs form at each end of the burn arc. A fully developed concave profile eventually results when the maneuver time is sufficiently long to place the solution on the threshold of region IVA of Fig. 4.

For an initial location exactly at the critical 1.7406 value, two BPs form with increasing maneuver time and move toward the ends, of the arc. As they reach the ends, a full BA forms with the thrust acceleration magnitude constant and equal to unity.

For an initial location at 1.9, greater than 1.7406, the solution develops differently. After the two initial BPs move down the sides of the constraint toward the ends of the burn arc, subsequent surface contacts result in an ever lengthening BA centered at (0, 1). This leads to an ITA in the central portion of the burn arc. For this case the thrust acceleration magnitude is convex, having its smallest magnitude near the center of the burn arc, in sharp contrast to the concave behavior shown in Fig. 9c. The largest maneuver time that leaves the initial and terminal thrust acceleration magnitude at a maximum on the second burn arc represents the threshold of region IVB solutions.

Region IV Solutions

If the maneuver time is sufficiently long, the solutions, as shown in Fig. 4, lie in region IV and are characterized by BAs in conjunction with ITAs. The ITAs exist for the entire duration of the second burn arc, and are characterized by intermediate thrust acceleration magnitudes that are less than the maximum value (except possibly at points on the region III/IV boundary).

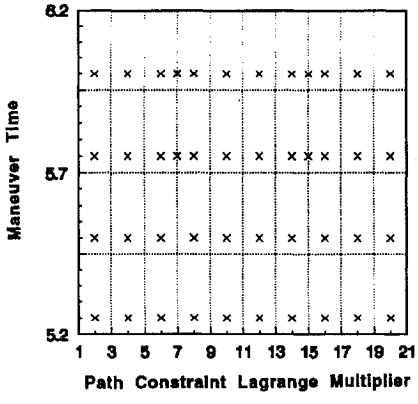

a) Active path constraints

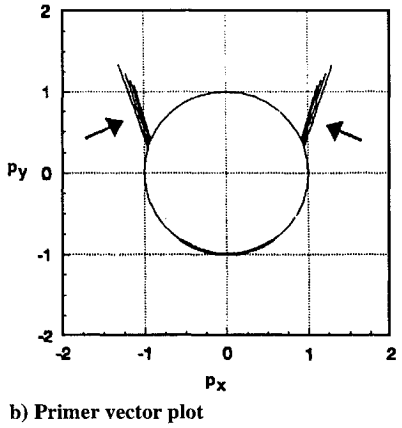

b) Primer vector plot

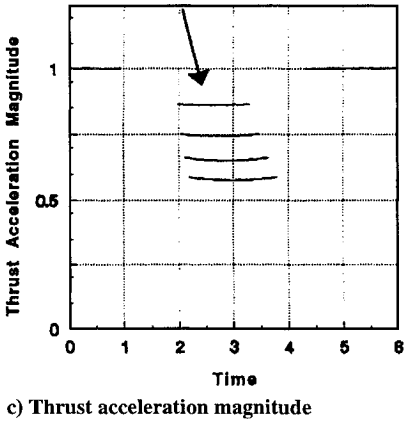

c) Thrust acceleration magnitude

Fig. 10 Region IV type solutions with initial position = 1.7 and maneuver times increasing from 5.25.

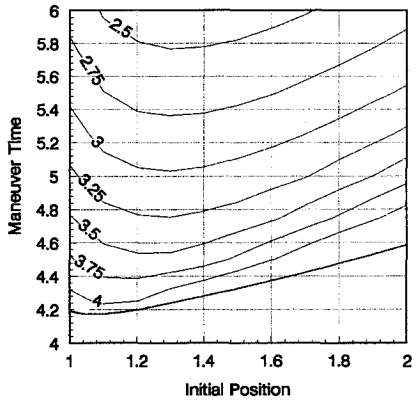

Fig. 11 Contour plot of symmetric rendezvous cost for maneuver time vs initial position; bottom curve is minimum-time solution.

Figure 10 displays information for an initial position at 1.7 and a maneuver time sufficiently long to place the solution in region IV. Note that the intermediate thrust acceleration history changes from a constant value to a convex profile. Because the initial position of 1.7 is less than the critical value of 1.7406, one might expect the profile to be concave, as in Fig. 9c. However, in Fig. 10b the maneuver time becomes sufficiently long to cross the line separating regions IVA and IVB. This line represents solutions with constant intermediate thrust acceleration profiles.

Cost Values

Figure 11 shows plots of total cost, defined by Eq. (3), as a function of initial position for various maneuver times. An interesting and somewhat unexpected result is apparent. As the spacecraft initial position moves closer to the constraint surface, the cost goes through a minimum value and begins to increase. In fact, for the given segmentation, the global minimum-time solution for a maximum thrust acceleration of unity occurs at an initial position of 1.072126 and a maneuver time (and cost) equal to 4.173908. This point is on the bottom curve in Fig. 11 (which is also the upper boundary of region I in Fig. 4) along which the cost is equal to the transfer time. An explanation for this apparent paradox is that for an initial position very close to the constraint, the spacecraft has to turn through a sharper angle to reach the destination point and, in doing so, expends more fuel. Thus, for a specified maneuver time there exists an optimum initial location.

It is of interest to compare the result in Fig. 11 with the optimal impulsive solutions reported by Taur et al. in Fig. 4 of Ref. 11. The optimal impulsive solution in field-free space is determined analytically, and a similar phenomenon occurs. For a given number of impulses the cost is a minimum at a particular initial position, and increases as one moves closer to the constraint. For the 10-impulse solution (the maximum number of impulses considered) the initial position for minimum cost is approximately 1.4.

General Rendezvous

Numerous solutions have been obtained for nonsymmetric rest-to-rest rendezvous and for nonsymmetric cases in which the terminal states are not at rest.[13] One such solution will be described here as an illustrative example. At the initial location of (1.5, 0) the spacecraft has an initial velocity toward the origin of (−0.5, 0). The specified final position is (−1.06, 1.06) with a final velocity (−0.177, −0.177) and the specified maneuver time is 4.85. The optimal solution has three burn arcs including an intermediate thrust with an approximately constant thrust acceleration magnitude. The path constraint Lagrange multipliers indicate a BA also exists. The magnitude of the last Lagrange multiplier is 10 times the others, indicating that the last contact point on the trajectory has a very large influence on the cost.

Conclusions

A comprehensive solution for rest-to-rest minimum-fuel rendezvous in field-free space has been obtained in the vicinity of a circular path constraint. Hermite–Simpson transcription proved to

be a very powerful tool for solving the optimal control problem. Using this direct method the resulting NLP Lagrange multipliers, which are discrete representations of the costate variables, provide valuable information that can be used to validate or invalidate the solution using the necessary conditions. In doing so, the benefits of an indirect method can also be realized. In the optimal trajectory problem the necessary conditions are provided by primer vector theory.

In all of the rendezvous cases examined, a number of basic characteristics were discovered.

1) The maximum allowed maneuver time is the optimal value.

2) The optimal number of burn arcs is three, separated by two coast arcs.

3) Intermediate thrusts occur only on the second burn arc.

4) BPs, accompanied by primer rate discontinuities, occur on the second burn arc.

5) Discontinuities in the Hamiltonian function rarely exist. The only jumps encountered were for initial points on the constraint boundary.

All symmetric, rest-to-rest solutions in the vicinity of the constraint are comprehensively identified, and fall into four distinct classes: 1) infeasible cases in which the spacecraft cannot perform the maneuver in the allotted time with the given thrust level; 2) single BP cases, in which the trajectory touches the constraint surface once, halfway through the maneuver in both position and time, with constant, maximum thrust acceleration; 3) transition cases, in which the trajectory touches the constraint surface multiple times, and may use an intermediate thrust level for a finite duration; and 4) BAs for which the trajectory rides the constraint surface for the entire duration of the second burn arc, using intermediate levels of thrust acceleration.

The initial position of 1.740602354434 for a unit radius constraint is a critical location where the curvature of a developing intermediate thrust arc for increasing maneuver time is zero. Initial positions for smaller or larger values of initial location will develop negative and positive curvatures, respectively, for the ensuing intermediate thrust.

For a specified maneuver time there exists an optimal value of initial position.

Appendix: Unconstrained Solution

The symmetric rest-to-rest problem without the path constraint is quite simple. The optimal solution is bang–bang thrust along a straight line from $x(0) = a > 0$ to $x(T) = -a$. For a maximum thrust acceleration magnitude of unity, the minimum time T_m for a solution to exist is easily shown to be given by $T_m^2 = 8a$ with a thrust history of $\Gamma = -1$ for $0 \le t < \frac{1}{2}T_m$ and $\Gamma = +1$ for $\frac{1}{2}T_m < t \le T_m$. The cost J is identical to T_m for this case. For $a = 1.7$ as in Figs. 6 and 7, the value of the cost in the unconstrained case is $J = 3.6878$.

For transfer times greater than T_m a coast period during which the engine is off is optimal. It is convenient to analyze a burn-coast-burn thrust sequence even though there are an infinite number of sequences of alternating burn and cost arcs that yield solutions of the same cost. Denoting the duration of each of the two burn arcs by t_b and the duration of the coast arc by t_c, for a specified value of $T > T_m$ it is necessary that

$$2t_b + t_c = T \tag{A1}$$

and that the total distance traveled from in going from rest to rest is $2a$:

$$t_b^2 + t_b t_c = 2a \tag{A2}$$

The desired solution to Eqs. (A1) and (A2) is obtained by selecting the appropriate algebraic sign in the quadratic solution to yield

$$t_b = \tfrac{1}{2}\left[T - (T^2 - 8a)^{\frac{1}{2}}\right] \tag{A3}$$

with

$$t_c = (T^2 - 8a)^{\frac{1}{2}} \tag{A4}$$

and a cost

$$J = 2t_b = T - (T^2 - 8a)^{\frac{1}{2}} \tag{A5}$$

As the value of T is increased, the duration of the coast arc monotonically increases and the cost monotonically decreases with $J \to 0$ as $T \to \infty$.

Acknowledgments

This research was supported in part by NASA Grants NAG3-805 and NAG3-1138 administered by NASA Lewis Research Center.

References

[1]Lawden, D. F., *Optimal Trajectories for Space Navigation*, Butterworths, London, 1963.

[2]Gobetz, F. W., and Doll, J. R., "A Survey of Impulsive Trajectories," *AIAA Journal*, Vol. 7, No. 5, 1969, pp. 801–834.

[3]Prussing, J. E., and Chiu, J.-H., "Optimal Multiple-Impulse Fixed-Time Rendezvous Between Circular Orbits," *Journal of Guidance, Control, and Dynamics*, Vol. 9, No. 1, 1986, pp. 17–22.

[4]Prussing, J. E., Wellnitz, L. J., and Heckathorn, W. G., "Optimal Impulsive Time-Fixed, Direct-Ascent Interception," *Journal of Guidance, Control, and Dynamics*, Vol. 12, No. 4, 1989, pp. 487–494.

[5]Jezewski, D. J., and Faust, N. L., "Inequality Constraints in Primer Optimal N-Impulse Solutions," *AIAA Journal*, Vol. 9, No. 4, 1971, pp. 760–763.

[6]Brusch, R. G., "Constrained Impulsive Trajectory Optimization for Orbit-to-Orbit Transfer," *Journal of Guidance and Control*, Vol. 2, No. 3, 1979, pp. 204–212.

[7]Stern, S. A., and Fowler, W. T., "Path-Constrained Maneuvering Near Large Space Structures," *Journal of Spacecraft and Rockets*, Vol. 22, No. 5, 1985, pp. 548–553.

[8]Soileau, K. M., and Stern, S. A., "Path-Constrained Rendezvous: Necessary and Sufficient Conditions," *Journal of Spacecraft and Rockets*, Vol. 23, No. 5, 1986, pp. 492–498.

[9]Prussing, J. E., and Clifton, R. S., "Optimal Multiple-Impulse Satellite Evasive Maneuvers," *Journal of Guidance, Control, and Dynamics*, Vol. 17, No. 3, 1994, pp. 599–606.

[10]Taur, D.-R., "Optimal, Impulsive, Time-Fixed Orbital Rendezvous and Interception with Path Constraints," Ph.D. Thesis, Dept. of Aeronautical and Astronautical Engineering, Univ. of Illinois, Urbana–Champaign, IL, June 1989.

[11]Taur, D.-R., Coverstone-Carroll, V., and Prussing, J. E., "Optimal Impulsive Time-Fixed Orbital Rendezvous and Interception with Path Constraints," *Journal of Guidance, Control, and Dynamics*, Vol. 18, No. 1, 1995, pp. 54–60.

[12]Groble, M. E., "A Preliminary Study of Optimal Maneuvers Near Large Space Structures," M.S. Thesis, Dept. of Aeronautical and Astronautical Engineering, Univ. of Illinois, Urbana–Champaign, IL, Jan. 1990.

[13]Wenzel, R. S., "Optimal Thrust-Limited Path-Constrained Rendezvous Using Hermite–Simpson Transcription and Nonlinear Programming," M.S. Thesis, Dept. of Aeronautical and Astronautical Engineering, Univ. of Illinois, Urbana–Champaign, IL, Jan. 1991.

[14]Marec, J.-P., *Optimal Space Trajectories*, Elsevier Scientific, Amsterdam, 1979.

[15]Enright, P. J., and Conway, B. A., "Discrete Approximations to Optimal Trajectories Using Direct Transcription and Nonlinear Programming," *Journal of Guidance, Control, and Dynamics*, Vol. 15, No. 4, 1992, pp. 994–1002.

[16]Hargraves, C. R., and Paris, S. W., "Direct Trajectory Optimization Using Nonlinear Programming and Collocation," *Journal of Guidance, Control, and Dynamics*, Vol. 10, No. 4, 1987, pp. 338–342.

[17]Bryson, A. E., Jr., and Ho, Y.-C., *Applied Optimal Control*, Hemisphere, New York, 1975.

[18]Gill, P. E., Murray, W., Saunders, M. A., and Wright, M. H., "User's Guide for NPSOL (Version 4.0): A Fortran Package for Nonlinear Programming," Systems Optimizations Lab., Dept. of Operations Research, TR SOL 86-2, Stanford Univ., Stanford, CA, Jan. 1986.

[19]Peressini, A. L., Sullivan, F. E., and Uhl, J. J., Jr., *The Mathematics of Nonlinear Programming*, Springer–Verlag, Berlin, 1988.